

Key Points:

- This study differentially quantifies the impacts of aerosol loading and properties and meteorology on scattering at three sites in China
- Scattering of light by aerosol is most sensitive to particle hygroscopicity and mass in Nanjing and humidity in Beijing
- Humidity substantially affects scattering during heavy haze in Beijing, whereas particle mass is more impactful in Nanjing and Guangzhou

Correspondence to:

Z. Li,
zhanqing@umd.edu

Citation:

Jin, X., Li, Z., Wu, T., Wang, Y., Su, T., Ren, R., et al. (2022). Differentiating the contributions of particle concentration, humidity, and hygroscopicity to aerosol light scattering at three sites in China. *Journal of Geophysical Research: Atmospheres*, 127, e2022JD036891. <https://doi.org/10.1029/2022JD036891>

Received 5 APR 2022
Accepted 12 NOV 2022

Author Contributions:

Conceptualization: Xiaoi Jin, Zhanqing Li
Data curation: Xiaoi Jin, Tong Wu, Yuying Wang
Formal analysis: Xiaoi Jin
Funding acquisition: Xiaoi Jin, Zhanqing Li
Investigation: Xiaoi Jin, Tong Wu, Yuying Wang, Rongmin Ren, Hao Wu, Dongmei Zhang, Shangze Li
Methodology: Xiaoi Jin, Tianning Su
Project Administration: Zhanqing Li
Writing – original draft: Xiaoi Jin
Writing – review & editing: Xiaoi Jin, Zhanqing Li, Tianning Su, Maureen Cribb

© 2022. The Authors.

This is an open access article under the terms of the [Creative Commons Attribution License](https://creativecommons.org/licenses/by/4.0/), which permits use, distribution and reproduction in any medium, provided the original work is properly cited.

Differentiating the Contributions of Particle Concentration, Humidity, and Hygroscopicity to Aerosol Light Scattering at Three Sites in China

Xiaoi Jin¹, Zhanqing Li² , Tong Wu³, Yuying Wang⁴, Tianning Su², Rongmin Ren³, Hao Wu⁵, Dongmei Zhang³, Shangze Li³, and Maureen Cribb²

¹State Key Laboratory of Subtropical Silviculture, Zhejiang A&F University, Hangzhou, China, ²Department of Atmospheric and Oceanic Science and ESSIC, University of Maryland, College Park, MD, USA, ³State Key Laboratory of Remote Sensing Science, College of Global Change and Earth System Science, Beijing Normal University, Beijing, China, ⁴Key Laboratory for Aerosol-Cloud-Precipitation of China Meteorological Administration, School of Atmospheric Physics, Nanjing University of Information Science and Technology, Nanjing, China, ⁵Plateau Atmosphere and Environment Key Laboratory of Sichuan Province, College of Atmospheric Science, Chengdu University of Information Technology, Chengdu, China

Abstract The scattering of light by aerosol particles dictates atmospheric visibility, which is a straightforward indicator of air quality. It is affected by numerous factors, such as particle number size distribution, particle mass concentration (PM_{2.5}), ambient relative humidity (RH), and chemical composition. The latter two factors jointly influence the aerosol liquid water content (ALWC). Here, the particle backscattering coefficient (β_p) under ambient RH conditions is investigated to differentiate and quantify the contributions of aerosol properties and meteorology using comprehensive observational datasets acquired at three megacities in China, that is, Beijing (BJ), Nanjing (NJ), and Guangzhou (GZ). Overall, the temporal variations in β_p under ambient RH conditions are consistent with those in ALWC at the three sites. The PM_{2.5} in BJ is systematically higher than in NJ and GZ, while ambient RH and aerosol hygroscopicity in NJ are much higher than in BJ and GZ. Notable differences in the variations of β_p with related factors at the three sites are demonstrated. β_p is more sensitive to particle hygroscopicity and mass in NJ and ambient RH in BJ. The relative contributions of these factors to β_p at the three sites under different pollution conditions are differentiated and quantified. The factor with the largest impact on the variability in β_p shifts from particle mass to ambient RH as air quality deteriorated to heavy pollution in BJ. The opposite is true in NJ. In GZ, the contributions of these factors to changes in β_p under different pollution conditions are similar, both dominated by PM_{2.5}.

Plain Language Summary Scattering of light by aerosol is a straightforward measure of air quality because of its close link to visibility. It is dictated primarily by aerosol mass loading, size distribution, chemical composition, and humidity. We used comprehensive observational datasets acquired at three sites in China to differentiate and quantify the contributions to the scattering of light by aerosol loading measured by aerosol particulate mass and aerosol properties, as well as humidity. The findings differ among the three cities due to differences in aerosol properties and meteorology. Scattering of light by aerosol is more sensitive to particle hygroscopicity and mass concentration in Nanjing and more sensitive to ambient humidity in Beijing. Local emission control measures can effectively reduce aerosol mass concentrations in Nanjing and Guangzhou. Weather conditions are more influential in Beijing due to the dominant influence of humidity.

1. Introduction

With the rapid development of China's economy, particulate pollution has become a common environmental issue. Severe haze events can endanger human health and impact local atmospheric visibility through aerosol direct radiative effects (Li et al., 2016; Su, Li, Zheng, et al., 2020; Y. Wang et al., 2017). However, the uncertainty of aerosol climate effects remains high due to the highly limited understanding of aerosol properties and their interactions with radiation, clouds, and precipitation, among others (IPCC, 2013; Stocker et al., 2013; Su, Li, Li, et al., 2020; Zhao et al., 2022).

The core problem of severe particulate pollution is the scattering of light by aerosol particles, affected by both pollutants (e.g., aerosol concentration, aerosol chemical species, and particle mixing state) (Covert et al., 1972; Pierangelo et al., 2004; L. Zhang et al., 2010) and meteorological factors (e.g., ambient relative humidity, RH)

(Hegg et al., 2002; McMurry, 2000). Under dry conditions, typically for ambient RH levels lower than 40%, aerosol concentration plays the most important role in determining aerosol optical properties, followed by the aerosol particle number size distribution (PNSD) and particle shape (Covert et al., 1972). Under high ambient RH conditions, the absorption of moisture by aerosol particles increases due to the hygroscopic particle components formed, for example, secondary aerosols (SA). Consequently, the aerosol liquid water content (ALWC) significantly increases as ambient humidity increases depending on the aerosol chemical composition and mixing state. Numerous studies have reported that ALWC can contribute greatly to particle mass, comprising more than 50% of fine particles when ambient RH levels are greater than 70% (Bian et al., 2014; Jin et al., 2020; McMurry, 2000; Zhang & McMurry, 1993). Particles absorb water through hygroscopic growth, changing particle sizes, shapes, and inhomogeneities, thus enhancing the scattering of light by aerosol. This is because a large number of particles smaller than 1 μm grow as the ambient RH increases, becoming larger particles ranging in size from 0.5 to 1 μm , which is more efficient for light scattering (Seinfeld & Pandis, 1998). Moreover, ALWC, which provides the medium for multiphase chemistry, can also facilitate the formation of SA, further enhancing the scattering of light by aerosol and influencing the aerosol direct radiative effect. Aerosol hygroscopic growth due to the enhanced aerosol hygroscopicity and the increase in humidity thus become the dominant factors influencing aerosol optical properties under high ambient humidity conditions. Hegg et al. (2002) reported the RH dependence on the scattering of light by aerosol from three experimental venues over the Pacific Ocean. Tao et al. (2014) differentiated between ambient- and dry-state single-scattering albedos and their diurnal variations, which are highly sensitive to ambient humidity. Cheng et al. (2008) reported that particle scattering properties are highly dependent on environmental humidity and further investigated the impact of the swelling effect on the interaction between aerosols and radiation in the Pearl River Delta region. The considerable increase in the aerosol scattering coefficient (σ_{sp}) under ambient RH conditions caused by the hygroscopic effect was demonstrated by Yoon and Kim (2006). Understanding how these related factors (aerosol mass concentration, PNSD, hygroscopicity, and ambient RH) affect aerosol optical properties under different ambient conditions is thus crucial to quantify the aerosol direct radiative effect.

Previous studies have mainly investigated the importance of particle mass and meteorological conditions (e.g., RH) in determining aerosol optical properties separately. Less focus has been placed on understanding their relative importance. Using abundant field measurements collected in three megacities in China (Beijing [BJ], Nanjing [NJ], and Guangzhou [GZ]), the aerosol backscattering coefficient (β_{p}) and its association with related impact factors (aerosol mass concentration, PNSD, hygroscopicity, and ambient RH) at these sites are differentiated and quantified in this study, helping identify factors contributing the most to changes in β_{p} under heavy pollution conditions. Both the methods and findings of this study are valuable for making sound policies in combating air pollution, especially in improving atmospheric visibility.

2. Data and Measurements

2.1. Sampling Sites

To understand the nucleation of aerosol particles, their hygroscopic growth and aging processes, and their impacts on particulate pollution, comprehensive field observations were carried out at three sites for specific time periods over several months (Figure 1): BJ (20 December 2018–10 February 2019), GZ (1 November 2019–31 January 2020), and NJ (1 November 2020–31 January 2021). A general description of the observation campaigns and instruments deployed can be found in Li et al. (2019). Table 1 summarizes the observational time periods at the three sites. Observations from each site cannot directly represent aerosol properties and the atmospheric environment of a city but are still representative to a certain extent. All sites are located in eastern China, the most densely populated region of China, which has experienced rapid economic development in recent years. As a result, it is also an area with high emissions of aerosol gaseous precursors and primary particles, leading to heavy air pollution. The observation site in BJ is located in the southern suburbs of the city (39.81°N, 116.48°E), surrounded by the fifth Ring Road and industrial parks. Pollutants affecting the area include those from nearby industrial activities, traffic emissions, and transport from the southern part of the North China Plain (Ren et al., 2021; D. Zhang et al., 2022). The observation site in NJ is located in the northern suburban area of the city (32.20°N, 118.72°E), surrounded by several large-scale industries, for example, electric power, steel, and petrochemical plants. Industrial emissions are the primary source of atmospheric aerosol particles here. The site is surrounded by busy highways, so it is also affected by traffic emissions (Fan et al., 2021; D. Zhang et al., 2022). The observation site in

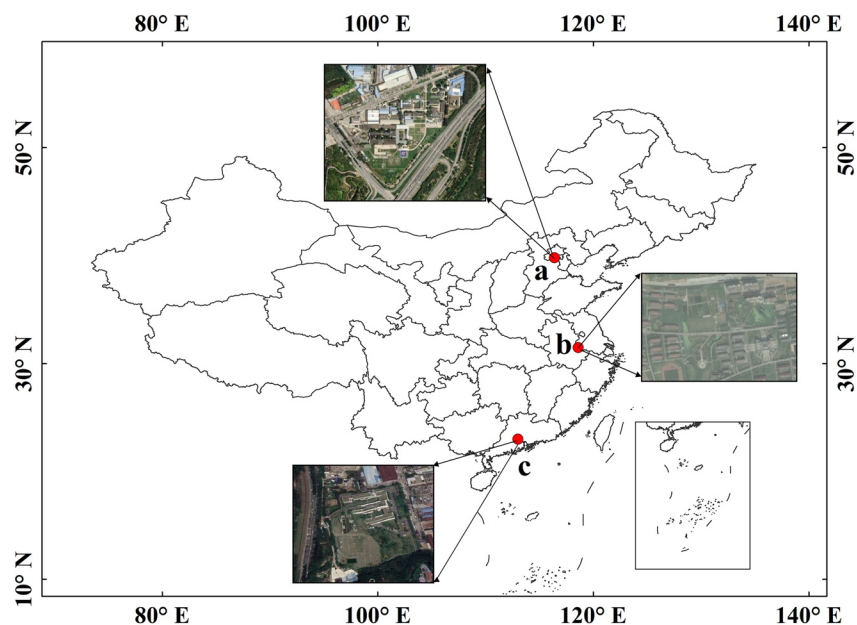


Figure 1. Locations of the three observation sites and images of their surroundings (inset figures): (a) Beijing, (b) Nanjing, and (c) Guangzhou.

GZ is located in the southwest suburban area of the city (23.01°N, 113.33°E) near one of the largest entertainment parks in China called Changlong Paradise. This site is affected by small factories, traffic emissions, and nearby cooking emissions from a night market (Jin et al., 2022; T. Wu et al., 2022).

2.2. Instrumentation at the Three Sites

Field measurements in BJ, NJ, and GZ were all carried out in a mobile container housing a set of instruments measuring various aerosol physical and chemical properties (Table 2), such as aerosol particle size by a Scanning Mobility Particle Sizer (SMPS), chemical species by an Aerosol Chemical Speciation Monitor (ACSM), and particle hygroscopicity by a Hygroscopicity Tandem Different Mobility Analyzer (H-TDMA), and a humidified nephelometer system (Aurora 3000, Ecotech). A particle mass concentration ($PM_{2.5}$) cyclone was installed outside the container near the entrance of the injector. Inside the container, the internal temperature was maintained at $\sim 20\text{--}25^\circ\text{C}$ using an air conditioner. A Nafion dryer (model PD-70T-24ss, Perma Pure Inc., USA) was used to keep the sampled air below 30% RH. A Li-COR 7500A system measured meteorological variables, such as air temperature (T), wind speed (WS) and direction (WD), atmospheric pressure, and RH. Quality-controlled $PM_{2.5}$ data came from real-time PM observational data provided by the China National Environmental Monitoring Center (China MEP, 2013).

The SMPS includes a DMA (model 3081A, TSI Inc.) and a condensation particle counter (model 3772, TSI Inc.) measuring PNSDs in the 10–600-nm size range at a 5-min time resolution.

The ACSM measures submicron non-refractory aerosol chemical components in real-time, mainly consisting of particulate ammonium (NH_4^+), sulfate (SO_4^{2-}), nitrate (NO_3^-), chloride (Cl^-), and organics (Org). The time resolution of the ACSM is 15 min. Pure ammonium nitrate is used to calibrate and determine the ionization efficiency of the ACSM following the processes described by Jimenez et al. (2003). Ng et al. (2011) and Y. Zhang et al. (2016) provide more detailed descriptions of the principle behind and the calibration of the ACSM. A seven-wavelength aethalometer (model AE-33, Magee Scientific Corp.) measures black carbon (BC) at a 5-min time resolution.

A humidified nephelometer system (Aurora 3000, Ecotech) measures aerosol optical properties at three wavelengths (450, 525, and 635 nm) at a 1-min time resolution and the hygroscopic enhancement factor at a 45-min time

Table 1
Observational Time Periods at the Three Sites

Site	Observational time period
BJ	12.20.2018–2.10.2019
NJ	11.01.2020–1.31.2021
GZ	11.01.2019–1.31.2020

Table 2
Instruments Deployed at Each Site

	Measurement	Time resolution	Measurement accuracy
SMPS	PNSD	5 min	Diameter: $\pm 3\%$; number: $\pm 5\%$
ACSM	Aerosol chemical composition	15 min	Org: $\pm 0.5 \mu\text{g m}^{-3}$; Inorg: $\pm 0.2 \mu\text{g m}^{-3}$
Aurora 3000	Light scattering (9° - 170°)	1 min	$\pm 2 \text{ Mm}^{-1}$
	Backscattering (90° - 170°)	1 min	$\pm 2 \text{ Mm}^{-1}$

resolution for one loop of RH ranging from 40% to 90%. Aerosol optical properties are measured under dry conditions (i.e., $\sigma_{\text{sp,dry}}$ and $\beta_{\text{p,dry}}$, Mm^{-1}) by a nephelometer. The ranges of observational angle in the measurements of $\sigma_{\text{sp,dry}}$ and $\beta_{\text{p,dry}}$ are 9° - 170° and 90° - 170° , respectively. $\beta_{\text{p,dry}}$ (Mm^{-1}) at 525 nm was used in this study. Using the corresponding hygroscopic enhancement factor, aerosol optical properties under ambient humidity conditions (i.e., $\sigma_{\text{sp,RH}}$ and $\beta_{\text{p,RH}}$) can be calculated. Here, $\beta_{\text{p,RH}}$ is used for further analysis.

3. Methodology

3.1. Hygroscopicity Parameter, κ

As proposed by Petters and Kreidenweis (2007), according to the Zdanovskii–Stokes–Robinson (ZSR) mixing rule, the particle hygroscopicity parameter κ can be calculated for an assumed internal mixture (Stokes & Robinson, 1966):

$$\kappa = \sum_i \varepsilon_i \kappa_i, \quad (1)$$

where ε_i denotes the volume fraction of the i th particle species, and κ_i represents the hygroscopicity parameter of the i th particle species. The hygroscopicity parameter κ is dimensionless. Previous studies based on field measurements and laboratory experiments have shown that the composition of submicron particles is dominated by Org, followed by NO_3^- , NH_4^+ , and SO_4^{2-} . The contributions of Cl^- and dust are negligible (Levin et al., 2014; Malm et al., 2009; Whitby, 1978; F. Zhang et al., 2014). Therefore, only Org, ammonium nitrate (NH_4NO_3), sulfuric acid (H_2SO_4), ammonium sulfate [$(\text{NH}_4)_2\text{SO}_4$], ammonium hydrogen sulfate (NH_4HSO_4), and BC were considered in this study. The aerosol hygroscopicity parameter here is thus the volume average of these six aerosol components. Using the mass concentrations of these species measured by the ACSM, the volume fraction of each species can be calculated as the ratio of the mass concentration to the corresponding density. The densities (g cm^{-3}) of Org, H_2SO_4 , $(\text{NH}_4)_2\text{SO}_4$, NH_4HSO_4 , NH_4NO_3 , and BC were assumed to be 1.4, 1.83, 1.76, 1.78, 1.725, and 1.7, respectively (Petters & Kreidenweis, 2007; Topping et al., 2005; Z. J. Wu et al., 2016). The κ values of Org, NH_4NO_3 , H_2SO_4 , $(\text{NH}_4)_2\text{SO}_4$, and NH_4HSO_4 were 0.1, 0.58, 1.19, 0.48, and 0.56, respectively (Mei et al., 2013; Nguyen et al., 2016; Y. Wang et al., 2017; Wex et al., 2009).

3.2. ALWC Simulations

The ALWC denotes the amount of liquid water contained in aerosol droplet particles, modeled here using the thermodynamic equilibrium model ISORROPIA II proposed by Fountoukis and Nenes (2007). Inputs to the model include inorganic species obtained from the ACSM and the corresponding ambient humidity and temperature. The model was set up to the reverse mode and in the metastable phase state. The simulated ALWC contains a certain degree of uncertainty incurred by neglecting the contribution of organic matter in the model (Fountoukis & Nenes, 2007). The Org species play a critical role in ultrafine particles smaller than 100 nm only, accounting for a few percent of the total water uptake (Gysel et al., 2007; Xue et al., 2016). Previous studies have validated results computed by the ISORROPIA II model with those computed from particle hygroscopicity measurements (Jin et al., 2022; Lin et al., 2014). The model assumes that the aerosol hygroscopicity has no effect on ambient vapor pressure and neglects the Kelvin effect in the κ -Köhler theory (Fountoukis & Nenes, 2007). This may influence the water uptake of the Aitken mode, but the influence is overall small (Zieger et al., 2017). Consequently,

Table 3

Sensitivity Test of $PM_{2.5}$ Thresholds for Determining Pollution Levels: $\frac{\text{threshold}_{+10} - \text{threshold}}{\text{threshold}}$

	Clean		Pollution		Heavy pollution	
β_p (Mm^{-1})	$-10 \mu g m^{-3}$	$+10 \mu g m^{-3}$	$-10 \mu g m^{-3}$	$+10 \mu g m^{-3}$	$-10 \mu g m^{-3}$	$+10 \mu g m^{-3}$
	1.9%	1.8%	1.2%	0.9%	1.8%	1.6%
RH (%)	0.38%	0.16%	0.69%	1.0%	1.2%	0.11%
κ	0.06%	0.16%	0.67%	0.28%	0.49%	0.12%

the water activity (a_w , %), defined as the effective mole fraction of water, is assumed to be equal to the ambient RH (Seinfeld & Pandis, 2006) in the model:

$$a_w = RH \quad (2)$$

According to the ZSR mixing rule, the ALWC ($\mu g m^{-3}$) can then be derived as (Stokes & Robinson, 1966):

$$ALWC = \sum_i \frac{M_i}{m_{0i}(a_w)} \quad (3)$$

where M_i and $m_{0i}(a_w)$ represent the mole concentration and the corresponding molality of the binary solution of the i th species under the same a_w with a complex solution, respectively. The ALWC values modeled by the ISOR-ROPIA II model here are thus used to gain insight into the influence of aerosol liquid water on the scattering of light by aerosol at the three sites.

3.3. The Contributions of Humidity, $PM_{2.5}$, and κ to Variations in β_p , RH

β_p is mainly influenced by the ambient humidity, aerosol particle accumulation ($PM_{2.5}$ and particle size distribution), and κ . The observational data were divided into three categories based on mass concentration and weather conditions: clean conditions ($PM_{2.5} < 75 \mu g m^{-3}$), polluted conditions ($75 \mu g m^{-3} < PM_{2.5} < 120 \mu g m^{-3}$), and heavily polluted conditions ($PM_{2.5} > 120 \mu g m^{-3}$) (Pan et al., 2018; Yang et al., 2021). Sensitivity tests of the $PM_{2.5}$ thresholds for dividing pollution levels were carried out. Table 3 shows that results based on different $PM_{2.5}$ mass concentrations are not sensitive to the thresholds. Based on the discussion in Section 4.3, the effect of particle size distribution on backscattering under the same ambient conditions (i.e., clean conditions) is very small. The contributions of humidity, particle mass concentration, and chemical composition to the variabilities in aerosol backscattering in these three categories can then be calculated (Cui et al., 2021; Huang & Yi, 1991). Briefly, β_p is expressed as a function of three parameters, that is, humidity, aerosol mass concentration, and chemical composition. The absolute changes in β_p due to RH ($\Delta\beta_p(RH)$), $PM_{2.5}$ ($\Delta\beta_p(PM)$), and κ ($\Delta\beta_p(\kappa)$) are calculated based on the control variable method. Specifically, the $PM_{2.5}$ mass concentration and κ are set to constant values, for example, $PM_{2.5} = 50 \mu g m^{-3}$ and $\kappa = 0.3$, to screen out ambient RH and β_p values under the same $PM_{2.5}$ and κ conditions based on all observational data. The absolute change in β_p due to ambient RH is calculated as

$$\Delta\beta_p(RH) = f(RH, PM_0, \kappa_0), \quad (4)$$

where PM_0 and κ_0 represent constant values of $PM_{2.5}$ mass concentration and κ , respectively. Similarly, the absolute change in β_p due to $PM_{2.5}$ mass concentration and κ can also be calculated:

$$\Delta\beta_p(PM) = f(RH_0, PM, \kappa_0), \quad (5)$$

$$\Delta\beta_p(\kappa) = f(RH_0, PM_0, \kappa), \quad (6)$$

where RH_0 represents constant values of RH. The relationships between β_p and $PM_{2.5}$ and β_p and κ are both linear, and that between β_p and ambient RH is exponential (Jin et al., 2022). Changes in β_p as a function of ambient humidity, particle mass concentration, and hygroscopicity can then jointly be expressed as:

$$\Delta\beta_p(RH, PM, \kappa) = a \cdot \Delta\beta_p(RH) + b \cdot \Delta\beta_p(PM) + c \cdot \Delta\beta_p(\kappa), \quad (7)$$

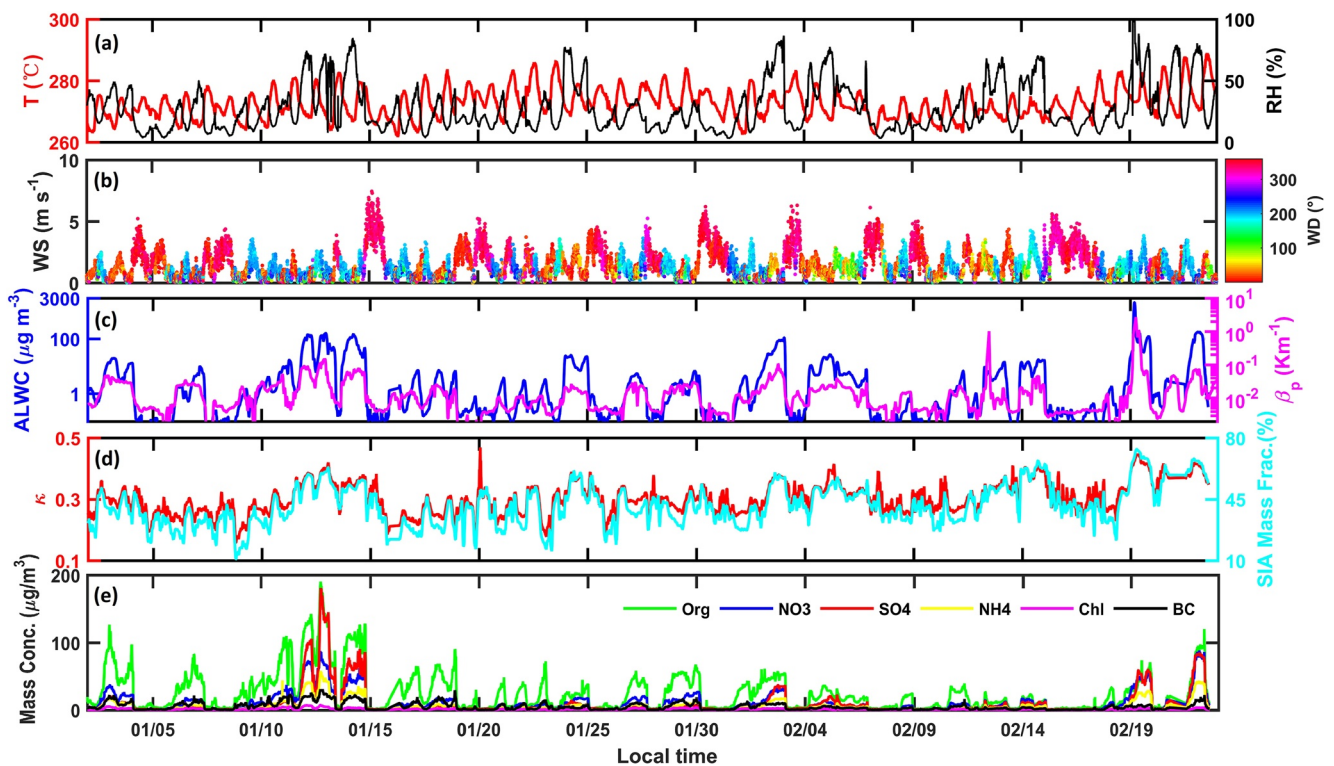


Figure 2. Time series of (a) air temperature (T) and ambient relative humidity (RH), (b) wind speed (WS, dots) and wind direction (WD, color of the dot), (c) aerosol liquid water content (ALWC) and aerosol backscattering coefficient (β_p), (d) aerosol hygroscopicity (κ) and secondary inorganics (SIA) mass fraction, and (e) mass concentrations of different aerosol chemical components in Beijing during the experiment.

Multiple linear regression is applied to deduce the corresponding coefficient of each parameter, that is, a , b , and c . Finally, the respective contributions of ambient humidity, aerosol mass concentration, and hygroscopicity to variations in backscattering can be calculated. Jin et al. (2022) provided detailed descriptions of the fitting and calculation processes.

4. Results and Discussion

4.1. Overview

Figures 2–4 show the time series of meteorological variables and aerosol-related parameters in BJ, NJ, and GZ. Ambient RH and T had significant diurnal variations at the three sites (Figures 2–4a). Diurnal changes in ambient RH and T in NJ were particularly small over periods of several days, with sustained high ambient humidity levels and small temperature fluctuations (Figure 3a). This is partly because RH in eastern China climatically increases with latitude (Xu et al., 2020). Figure 2b shows the time series of WS and the corresponding WD in BJ. When the prevailing WD was from the south, polluted air masses with high humidity were transported to BJ, fostering the rapid formation, growth, and aging of SA in BJ (Jin et al., 2020; Sun et al., 2012). However, clean and dry air masses were transported to BJ as the wind changed to strong northerly winds, facilitating the rapid removal of pollutants (Figures 2a and 2e). These results suggest that heavy haze and the local WD in BJ are highly correlated. This was not seen in NJ and GZ (Figures 3 and 4b). Figures 2–4c show the time series of ALWC and β_p at the three sites. The temporal changes in β_p are consistent with those in ALWC in BJ, NJ, and GZ, suggesting the significant impact of the hygroscopic effect of particles on aerosol backscattering (Kuang et al., 2016; Xu et al., 2020). Figure 5 shows the average values of β_p and ALWC at the three sites. On average, β_p in BJ was the highest ($54 \pm 68 \text{ Mm}^{-1}$), followed by that in NJ ($39 \pm 28 \text{ Mm}^{-1}$) and GZ ($30 \pm 17 \text{ Mm}^{-1}$) (Figure 5a). The average ALWC in NJ was $39 \pm 110 \mu\text{g m}^{-3}$, much higher than that in BJ ($15 \pm 75 \mu\text{g m}^{-3}$) and GZ ($9 \pm 10 \mu\text{g m}^{-3}$). Such a difference is expected to be jointly affected by the aerosol mass concentration, hygroscopicity, and ambient RH. Figure 6a shows that the average particle mass concentrations in BJ, NJ, and GZ were 56 ± 73 , 47 ± 28 , and

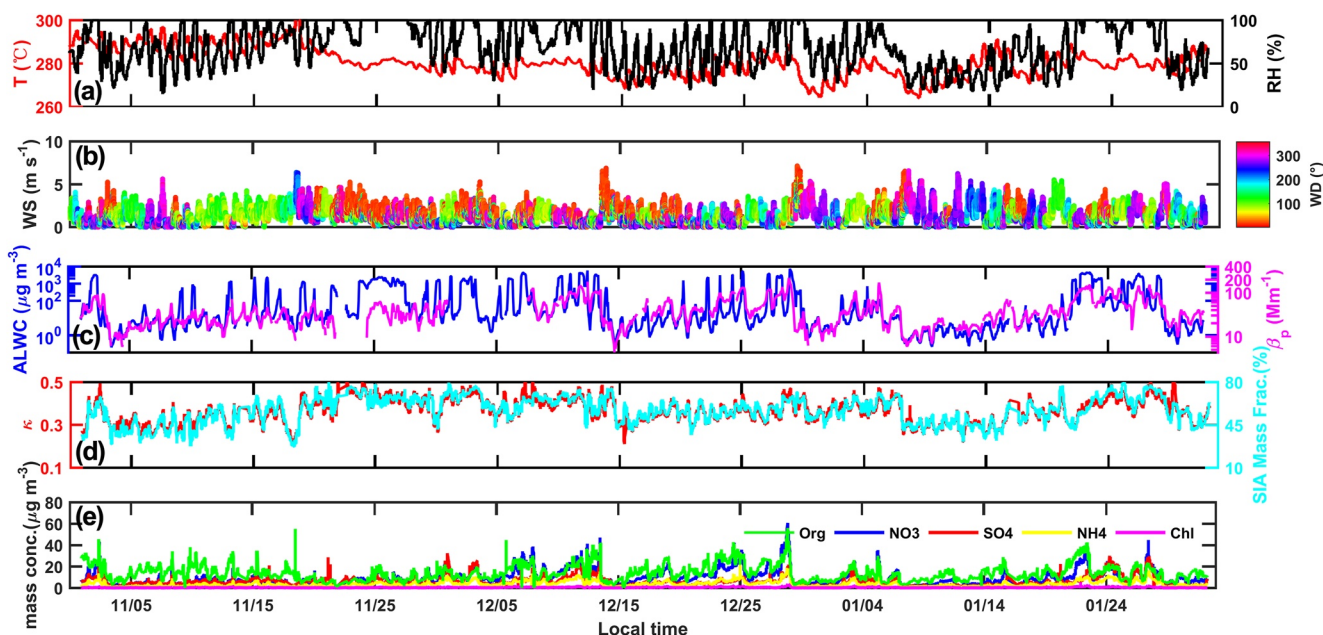


Figure 3. Same as Figure 2 but in Nanjing.

$43 \pm 26 \mu\text{g m}^{-3}$, respectively, illustrating more severe pollution conditions in BJ than in NJ and GZ. This is partly related to the outbreak of the COVID-19 epidemic that occurred during the sampling period in GZ, leading to lockdowns in China. The observational period in NJ was in the late stage of the epidemic when major entertainment venues, industries, and institutions had all opened normally. This suggests that controlling local emissions can effectively suppress pollution processes (X. Liu et al., 2008; Y. Wang et al., 2017). The ambient RH in NJ was systematically higher than in BJ and GZ (Figures 2–4a). The average RH in NJ was $70\% \pm 24\%$, much higher than in GZ ($54\% \pm 18\%$) and BJ ($27\% \pm 19\%$) (Figure 6b). Figure 6c shows the average aerosol hygroscopicity at

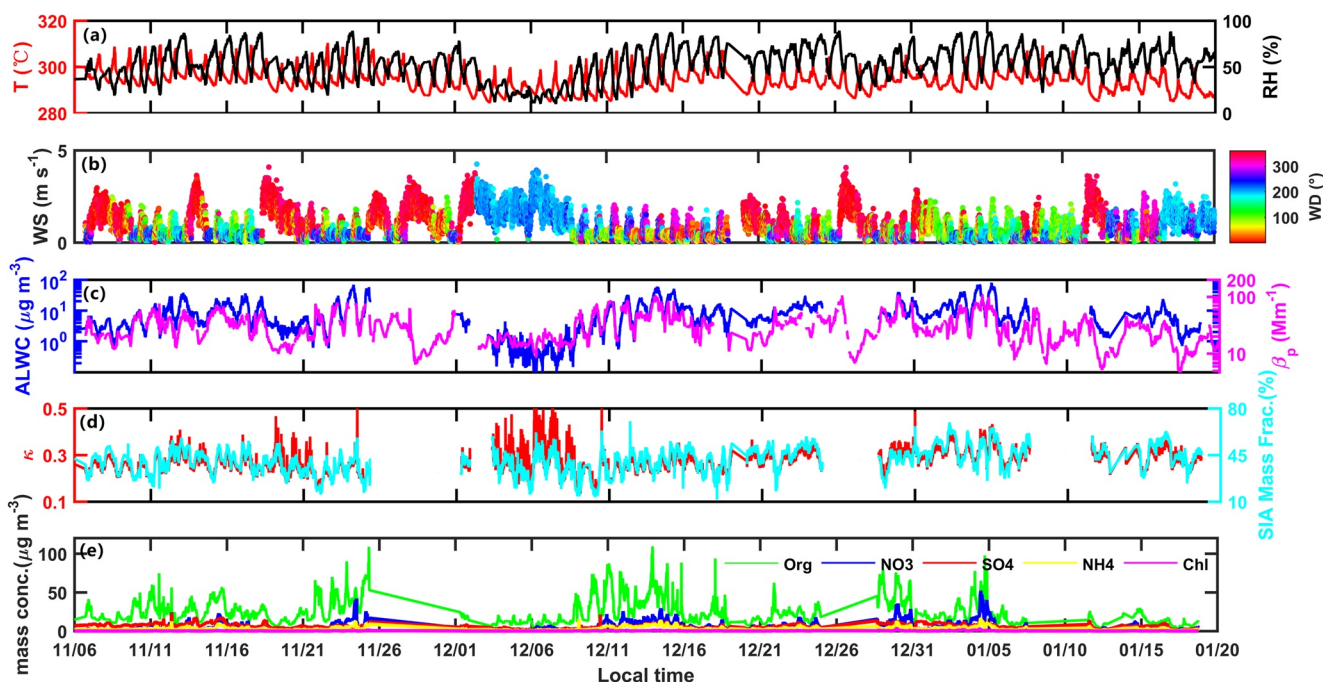


Figure 4. Same as Figure 2 but in Guangzhou.

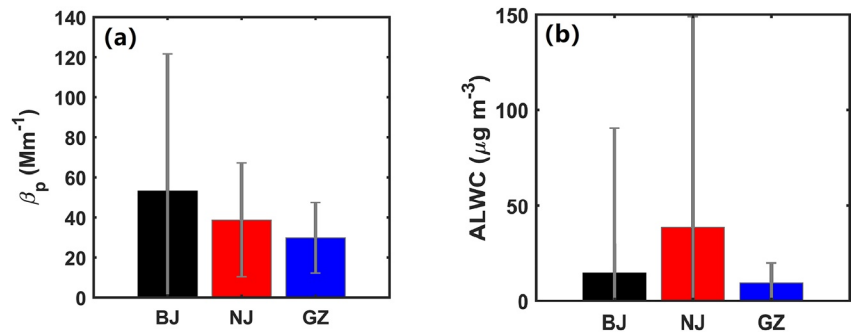


Figure 5. Average values and standard deviations of (a) aerosol backscattering coefficient (β_p) and (b) aerosol liquid water content (ALWC) at the three sites during their respective observational periods: Beijing (BJ), Nanjing (NJ), and Guangzhou (GZ).

the three sites, with the highest values in NJ (0.37 ± 0.06), followed by BJ (0.30 ± 0.06) and GZ (0.27 ± 0.05), suggesting differences in the aerosol chemical composition at the three sites.

Figures 2–4e show the time series of aerosol chemical composition (Org, SO_4^{2-} , NO_3^- , NH_4^+ , and Cl^-) in BJ, NJ, and GZ, respectively. Org dominated the $PM_{2.5}$ mass concentration, accounting for 52%, 40%, and 57% of the total mass concentrations in BJ, NJ, and GZ, respectively. The mass fractions of highly hygroscopic species, for example, SO_4^{2-} and NO_3^- , in NJ (31% and 18%, respectively) were much higher than in BJ (21% and 10%, respectively) and GZ (17% and 12%, respectively). Figures 2–4d show the time series of κ and secondary inorganics (SIA) mass fraction derived from the chemical composition at the three sites, illustrating that their respective trends agree well. This indicates the importance of the mass fraction of SIA in determining aerosol hygroscopicity. Accordingly, κ in NJ was much stronger than in BJ and GZ. Also observed in BJ was the gradual enhancement of κ as air pollution formed and ALWC and ambient RH increased (Figure 2). This is partly related to Henry's law and the positive feedback between κ and ALWC (Volkamer et al., 2007; Z. Wu et al., 2018). Henry's law as the driver would force reaching thermodynamic equilibrium, enhancing the aerosol swelling effect. So, with an increase in ambient humidity, the absorption of moisture by aerosol particles and the partitioning of gas-phase pollutants, such as dinitrogen pentoxide and sulfur dioxide, to the condensed phase is accelerated. A large number of SA formed through liquid-phase chemical reactions contribute to enhancing aerosol hygroscopicity. This phenomenon also occurred in NJ and GZ but not as significantly as in BJ. These results demonstrate the important effect of atmospheric chemical processes on aerosol backscattering, except for ambient humidity and the emission of primary particles. The ALWC is mostly influenced by ambient humidity and particle chemical components (Tan et al., 2017). The corresponding ALWC in NJ was the highest even though there was relatively light pollution and a lower particle mass concentration than in BJ. Note that the ALWCs in BJ and NJ had large standard deviations (Figure 5b), mainly affected by variations in aerosol mass concentration and ambient RH (Figure 6b). From Figures 5 and 6, RH in GZ was higher than in BJ, but ALWC was less than that in BJ. This is mainly caused by the combined impact of the low aerosol loading and weak hygroscopicity in GZ. This demonstrates that ALWC cannot easily form in a clean atmosphere and under weak hygroscopic conditions even

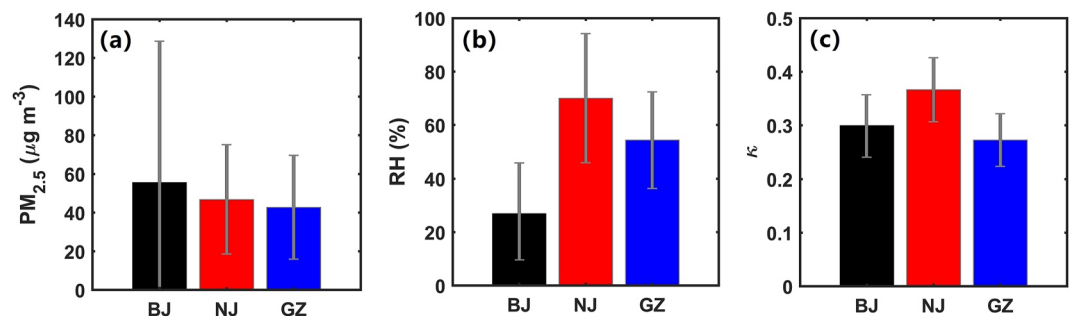


Figure 6. Average values and standard deviations of (a) $PM_{2.5}$ mass concentration, (b) ambient relative humidity (RH), and (c) aerosol hygroscopicity parameter (κ) at the three sites: Beijing (BJ), Nanjing (NJ), and Guangzhou (GZ).

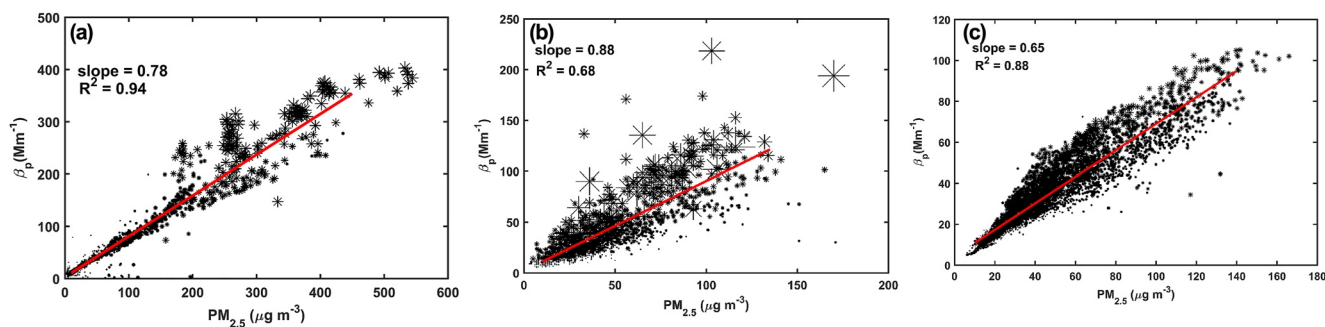


Figure 7. Aerosol backscattering coefficient (β_p) as a function of $PM_{2.5}$ mass concentration at the three sites: (a) Beijing (BJ), (b) Nanjing (NJ), and (c) Guangzhou (GZ). The red lines are the best-fit lines from linear regression. The slope of the best-fit line and the coefficient of determination are given in each panel. Increasing symbol sizes represent increasing aerosol liquid water contents.

though sufficient moisture is present for particles to absorb (Chen et al., 2014; Ma et al., 2014). This indicates that ALWC, affected by humidity, fine-mode particle concentration, and chemical composition, has a significant effect on the scattering of light by aerosol.

4.2. Correlation Analysis Between β_p and Aerosol Mass Concentration

Figure 7 shows the relationships between β_p and particle mass concentration differentiated by ALWC in BJ, NJ, and GZ. The coefficients of determination (R^2) between aerosol backscattering and particle mass concentration in BJ, NJ, and GZ are 0.94, 0.68, and 0.88, respectively. The aerosol backscattering correlates well with particle mass concentration in BJ and GZ but has a relatively weaker correlation in NJ. Such a difference is partly due to the influence of the hygroscopic growth process on aerosol backscattering. β_p gradually increases as ALWC increases under the same particle mass concentration conditions in BJ, NJ, and GZ. Furthermore, the increases were more significant as ALWC increased under high particle mass concentration conditions. However, as heavy haze events formed, the variation in β_p with ALWC differed in BJ, NJ, and GZ. Figure 7a shows that under low $PM_{2.5}$ mass concentration conditions in BJ, ALWC was very small, and β_p was highly correlated with the particle mass concentration. With the development of air pollution, a sharp rise in ALWC was observed (Figure 7a). This is likely because ALWC is mainly affected by ambient RH and aerosol hygroscopicity. In BJ, clean conditions are always accompanied by strong northerly winds that bring in clean, dry air masses (T. Wang et al., 2010). This is not conducive to the formation of ALWC. Polluted conditions are always accompanied by weak southerly winds that are associated with polluted, humid air masses, beneficial to the formation of SA and ALWC (T. Wang et al., 2010). These results suggest that ALWC is highly correlated with pollution in BJ. β_p in BJ is thus highly correlated with aerosol mass concentration, affected by ambient RH and aerosol hygroscopicity. The relatively weak correlation between aerosol scattering and mass concentration in NJ is caused by the high ambient humidity during the observational period. Note that the ALWC in NJ was as much as five times greater than in BJ (Figure 7b). Noticeably different from BJ, high ALWC values were observed during clean and polluted periods in NJ (Figure 7b), related to the high ambient RH levels observed under clean and polluted conditions (Figure 3a). The high uptake of liquid water by aerosol particles under low $PM_{2.5}$ mass concentration conditions would change their size and shape, further increasing the scattering of light by aerosol. Accordingly, β_p varied strongly under low aerosol mass concentration conditions, with the variation more significant under high aerosol mass concentration conditions in NJ, making the correlation between aerosol backscattering and aerosol particle mass concentration much weaker than in BJ. These results point to different formation mechanisms of pollution in BJ and NJ. The formation of heavy pollution in BJ is highly dependent on a high humidity environment, while in NJ, there was no such dependence on ambient humidity. Figure 7c shows that the ALWC in GZ was much lower than in BJ and NJ. This is likely linked to the much lower aerosol hygroscopicity during the sampling period in GZ, leading to a good correlation between β_p and aerosol loading in GZ. Particle hygroscopic growth is thus relatively weaker, and ALWC is not easily formed under clean conditions.

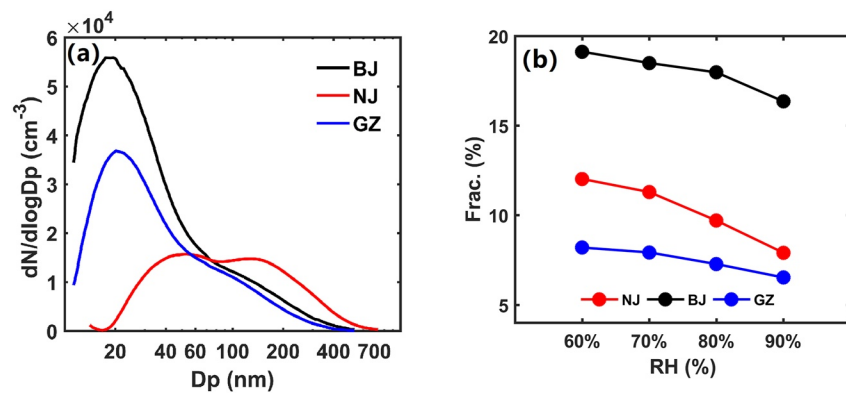


Figure 8. (a) Average aerosol particle number size distributions (PNSDs) and (b) average contributions of PNSDs to changes in aerosol backscattering coefficient at different relative humidity (RH) levels at the three sites: BJ, (black), NJ, (red), and GZ (blue).

4.3. Comparison of the Sensitivity of β_p to Related Factors in BJ, NJ, and GZ

4.3.1. The Impact of Particle Size Distribution on β_p

In addition to ambient humidity, particle concentration, and hygroscopicity, aerosol scattering is also affected by aerosol particle size distribution. Figure 8a shows the average PNSDs under dry conditions at BJ, NJ, and GZ. Note that the three PNSDs all had two peaks, but particle sizes and number concentrations corresponding to the two peaks differed among the three sites. Particles with diameters of ~40 nm denote locally emitted primary particles, and particles with diameters of ~150 nm represent regionally transported particles (Y. Wang et al., 2017; F. Zhang et al., 2017). In BJ and GZ, the average PNSDs had a single dominant peak at ~20 nm, suggesting large emissions of local small hydrophobic particles (e.g., traffic and cooking emissions) with externally mixed low hygroscopicity. However, the second peak in BJ (~150 nm) was larger than that in GZ (~100 nm), indicating more aged particles and consequently higher κ values in BJ. Number concentrations were the highest in BJ, particularly for small particles. Noticeably different from BJ and GZ, the average PNSD in NJ had dominant peaks at ~40 and ~150 nm, likely affected by a mixture of primary hydrophobic and secondary hygroscopic particles. Aerosol particles in NJ were thus much more hygroscopic than at the other two sites (also shown in Figure 6c).

The relative contributions of the particle size distribution to changes in backscattering according to Mie scattering theory at the three sites were examined next (Figure 8b) (Bohren & Huffman, 2007; Jin et al., 2022). All available observed PNSD data were first collected. The $\text{PM}_{2.5}$ and aerosol hygroscopicity values were both fixed, equal to their respective mean values at the three sites. Aerosol backscattering properties were then calculated according to Mie scattering theory based on the different PNSDs at each site. We defined the average contribution of the shape of the PNSD to changes in backscattering as the ratio of the standard deviation to the mean value of the calculated β_p derived from the three sites. Figure 8b shows the overall impact of the aerosol size distribution on aerosol backscattering for four different RH values at the three sites. The mean values of the contributions to aerosol backscattering in GZ were 8.19%, 7.92%, 7.27%, and 6.52% for RH levels 60%, 70%, 80%, and 90%, respectively. This demonstrates that the particle size distribution played a relatively weak role in influencing particle backscattering under the same particle mass concentration conditions during the sampling period in GZ. However, for BJ (NJ), the contributions were 19.24% (12.43%), 18.32% (10.62%), 17.68% (9.73%), and 16.12% (7.89%) for RH levels 60%, 70%, 80%, and 90%, respectively, much higher than in GZ. This indicates that the impact of particle size distribution on particle backscattering in BJ and NJ was much stronger than in GZ.

4.3.2. The Impact of RH and κ on Hygroscopic Growth

To further compare differences in the impact of RH and κ on hygroscopic growth among the three sites, average RH, κ , particle depolarization ratio (δ_p , dimensionless), PNSD, and average mass fractions of aerosol chemical components under clean, polluted, and heavily polluted conditions were examined (Figure 9). With the formation and development of pollution, the ambient RH and aerosol hygroscopicity gradually increased in BJ, reaching their highest values under heavy pollution conditions (Figure 9a). Correspondingly, a gradual decrease in δ_p was

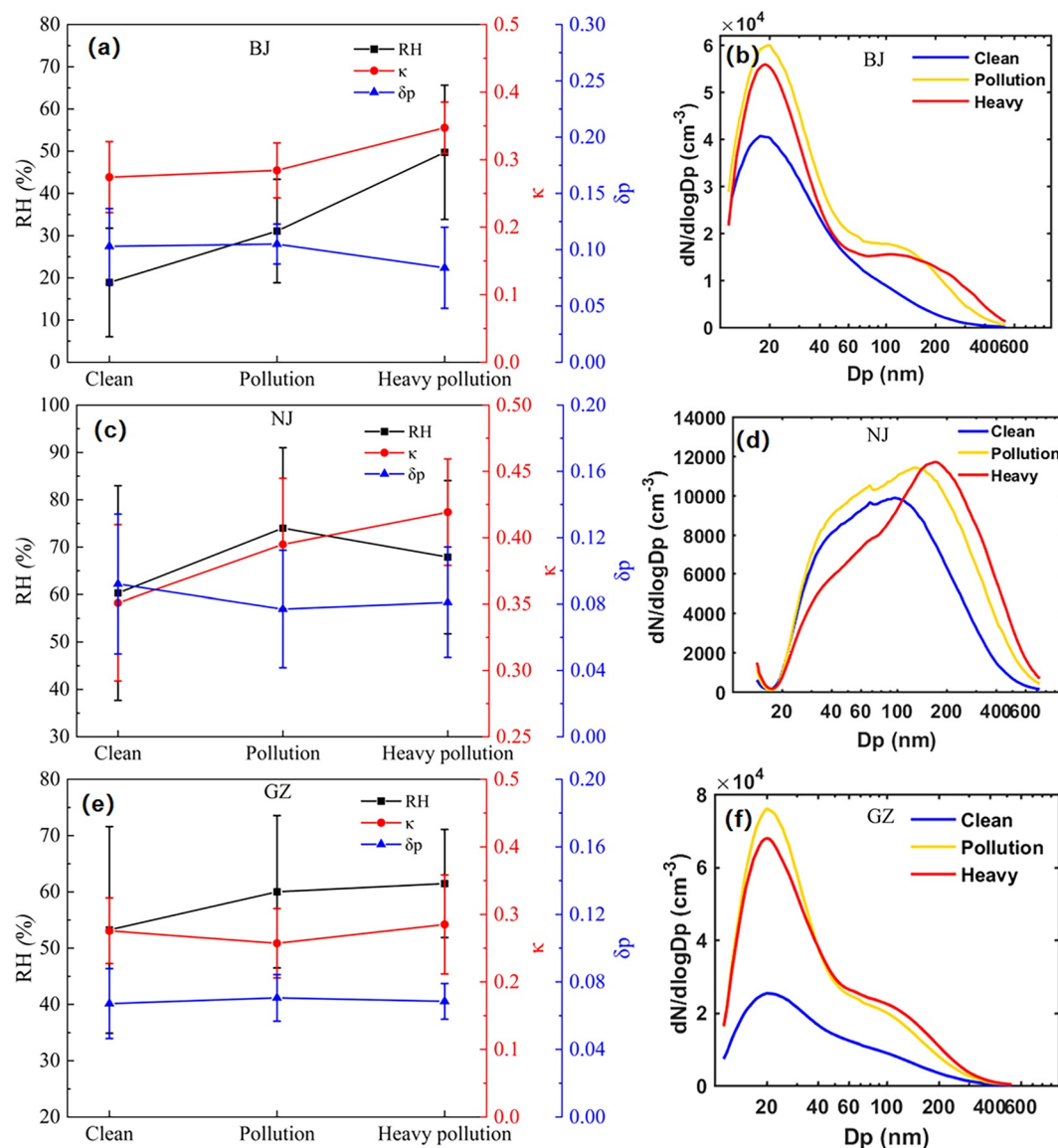


Figure 9. Average ambient relative humidity (RH), aerosol hygroscopicity parameter (κ), and depolarization ratio (δ_p) under different pollution conditions in (a) Beijing (BJ), (c) Nanjing (NJ), and (e) Guangzhou (GZ). Average aerosol particle number size distributions (PNSDs) under clean conditions (blue), polluted conditions (yellow), and heavily polluted conditions (red) in (b) BJ, (d) NJ, and (f) GZ.

observed (Figure 9a). Furthermore, the particle size corresponding to the smaller peak significantly increased from ~ 150 nm (polluted conditions) to ~ 200 nm (heavily polluted conditions) (Figure 9b). These results illustrate that with increasing RH, non-spherical hygroscopic particles gradually take up water and grow, becoming almost spherical, implying the important impact of RH and κ on hygroscopic growth. With an incremental change in ALWC, the phase state of aerosols may change from solid or semisolid to liquid, facilitating chemical reactions (Kuwata & Martin, 2012). Figure 10a shows that the mass concentration fractions of NO_3^- and SO_4^{2-} rose in BJ when going from clean to heavily polluted conditions. The corresponding PNSDs switched from having one peak at ~ 20 nm (clean conditions) to two peaks (polluted and heavily polluted conditions) (Figure 9b), indicating a change in emission source from local primary aerosols to a mixture of primary and aged particles. These together would lead to a rapid enhancement in extinction efficiency (Q_s), further enhancing the scattering of light by aerosol (Kuang et al., 2016; J. Liu et al., 2020; Y. Wang et al., 2017; Xu et al., 2020). Figure 9d shows that the dominant peaks of the PNSDs in NJ significantly changed from ~ 100 nm (clean conditions) to ~ 150 nm (polluted conditions) to ~ 200 nm (heavily polluted conditions). This is caused by the continuous formation of

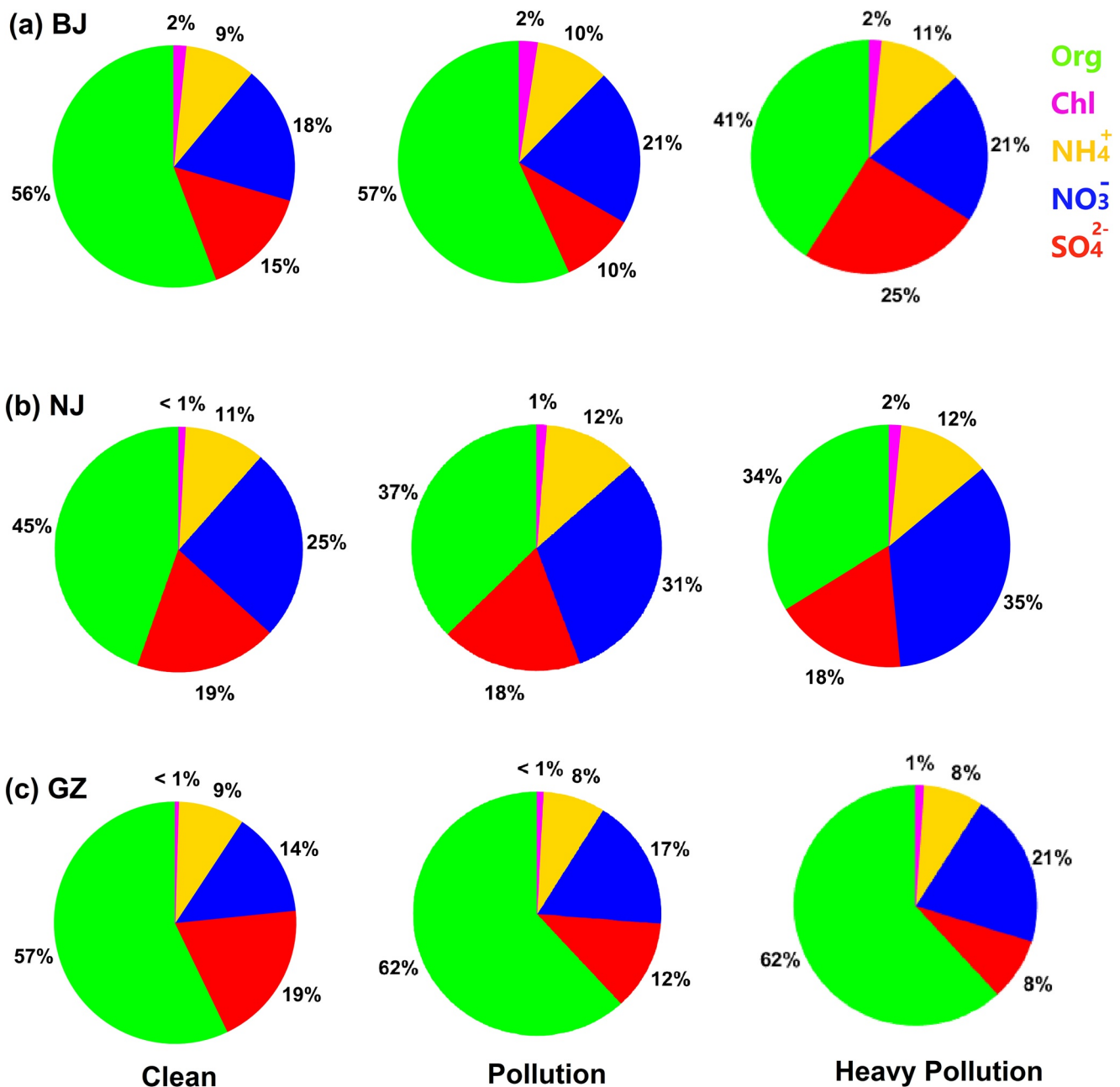


Figure 10. Average mass fractions of different aerosol chemical components under clean conditions (left column), polluted conditions (middle column), and heavily polluted conditions (right column) in (a) Beijing (BJ), (b) Nanjing (NJ), and (c) Guangzhou (GZ).

SA (e.g., SO_4^{2-} and NO_3^-) with larger particle sizes and stronger hygroscopicity during the development of pollution (Figure 10b). These results demonstrate that similar to BJ, RH and hygroscopicity in NJ also gradually increased with the development of pollution, resulting in particles becoming more spherical and larger (Figures 9c and 9d). Figures 9e, 9f and 10c show variations in δ_p , PNSD, and aerosol chemical composition with ambient RH and hygroscopicity under different pollution conditions in GZ. Overall, there was a slight increase in RH, hygroscopicity, and aerosol chemical components with the development of pollution compared with BJ and NJ. The PNSDs had similar patterns, with a dominant peak for small particles under clean and polluted conditions and with similar aerosol chemical compositions dominated by Org (Figure 10c). This shows that the aerosol hygroscopic growth had a relatively small influence on Q_s and backscattering at this site. In summary, the increases in RH and particle hygroscopicity significantly influence the aerosol size, shape, and chemical

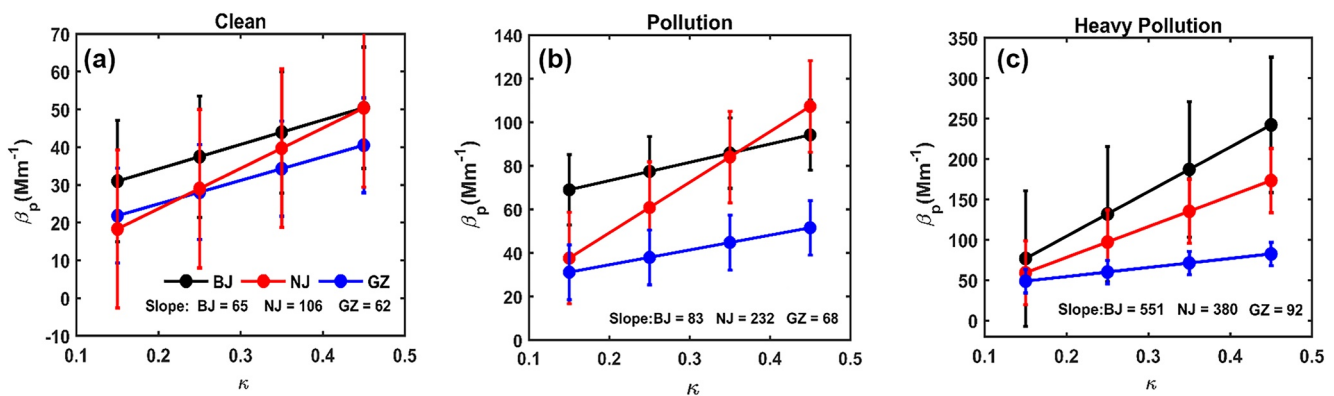


Figure 11. Absolute changes in aerosol backscattering coefficient (β_p) with aerosol hygroscopicity (κ) in Beijing (BJ), Nanjing (NJ), and Guangzhou (GZ) under (a) clean, (b) polluted, and (c) heavily polluted conditions. Slopes of the lines through the points are given in each panel.

composition through the hygroscopic growth process, which in turn affects Q_s and the scattering of light by aerosol particles.

4.3.3. Sensitivity of β_p to RH, $PM_{2.5}$, and κ

As discussed in Section 4.3.2, the impact of the PNSD shape on particle backscattering varied little under the same environmental conditions (e.g., polluted conditions) in BJ, NJ, and GZ. Also, as described in Section 4.2, the humidity, particle concentration, and chemical composition all significantly influenced aerosol backscattering. However, the averaged aerosol variables and their relative contributions to aerosol backscattering differed. Therefore, a quantitative evaluation of the influences of humidity, particle concentration, and chemical composition on aerosol backscattering under different pollution conditions in BJ, NJ, and GZ is needed.

Absolute variations in aerosol backscattering caused by κ (Figure 11), particle mass concentration (Figure 12), and ambient RH (Figure 13) under different pollution conditions in BJ, NJ, and GZ were derived using the methods described in Section 3.3. β_p changed linearly with particle mass concentration and hygroscopicity under clean and polluted conditions in BJ, NJ, and GZ (Figures 11–13). When κ increased by 0.1, β_p in BJ, NJ, and GZ increased by 6.5, 10.6, and 6.2 Mm^{-1} (clean), 8.3, 23.2, and 6.8 Mm^{-1} (polluted), and 55.1, 38.0, and 9.2 Mm^{-1} (heavily polluted), respectively (Figure 11). With the generation and development of pollution, aerosol scattering in BJ, NJ, and GZ became increasingly sensitive to hygroscopicity. Scattering of light by aerosol in NJ showed the strongest sensitivity to aerosol hygroscopicity under clean and polluted conditions, likely because there was more highly aged SA formed at that site compared with BJ and GZ, particularly under polluted conditions (e.g., NO_3^- mass fraction = 31%). The slope slightly increased in BJ because the NO_3^- mass fraction changed slightly, going from a mass fraction of 18% under clean conditions to 21% under polluted conditions. Note the jump in the slope in BJ under heavily polluted conditions, even higher than that in NJ, indicating the significant enhancement of aerosol hygroscopicity due to the explosive growth of a large amount of SO_4^{2-} with the development of

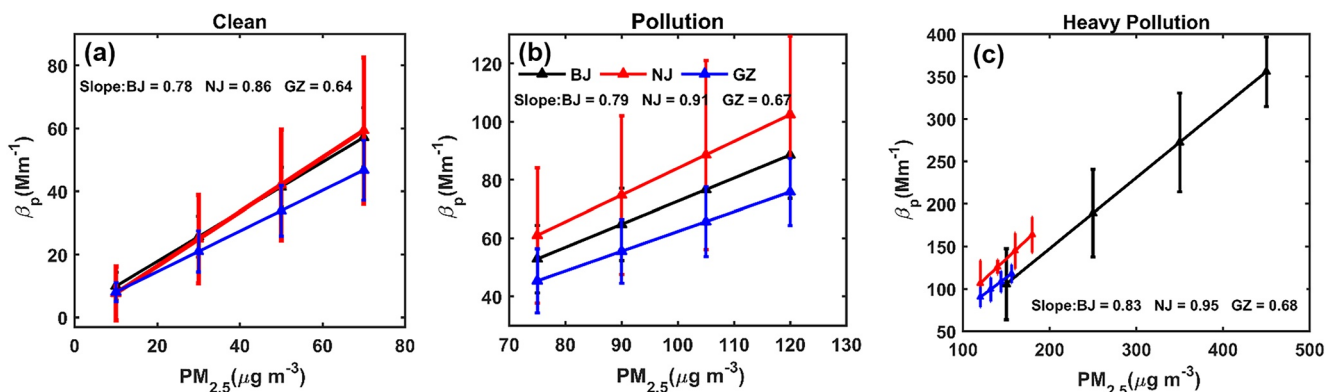


Figure 12. Same as Figure 11 except for absolute changes in aerosol backscattering coefficient (β_p) with $PM_{2.5}$ mass concentration.

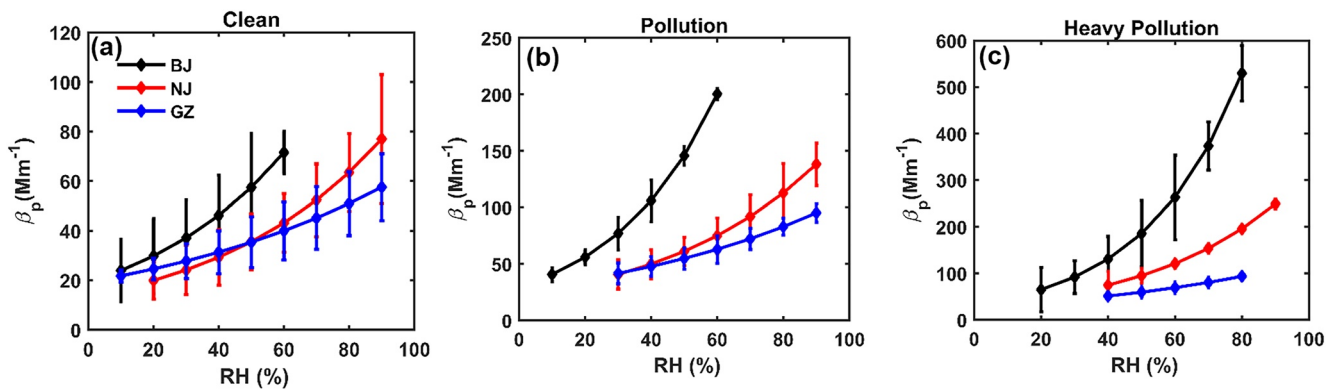


Figure 13. Same as Figure 11 except for absolute changes in aerosol backscattering coefficient (β_p) with ambient relative humidity (RH).

pollution (mass fraction increasing from 10% to 25%). The β_p in GZ showed a much weaker sensitivity to aerosol hygroscopicity as pollution levels increased, likely because the aerosol chemical composition dominated by Org changed little as more pollution formed.

Figure 12 shows that when $10 \mu\text{g m}^{-3}$ was added to the particle mass, β_p in BJ, NJ, and GZ increased by 7.8, 8.6, and 6.4 Mm^{-1} (clean), 7.9, 9.1, and 6.7 Mm^{-1} (polluted), and 8.3, 9.5, and 6.8 Mm^{-1} (heavily polluted), respectively. Compared with BJ and GZ, the influence of $\text{PM}_{2.5}$ mass concentration on β_p in NJ was the strongest under clean and polluted conditions. The steady rise of slopes in NJ with the development of pollution suggests the continuous formation of highly aged particles. The standard deviation of the particle mass concentration in BJ was smaller than that in NJ and GZ, mainly due to the stronger correlation between aerosol backscattering and fine-mode particle concentration in BJ. The slight increase in slope from clean to polluted conditions in BJ suggests a small enhancement of the sensitivity of particle backscattering to aerosol mass. The pronounced increase seen under heavily polluted conditions implies a shift in particle size distribution. β_p in GZ showed a much weaker sensitivity to aerosol mass, related to the relatively light level of pollution during the observational period at this site.

β_p changed exponentially with ambient humidity in BJ, NJ, and GZ, similar to how ALWC changed as ambient humidity increased (Jin et al., 2020, 2022), suggesting the significant influence of particle liquid water on aerosol backscattering. Figure 13 shows that the sensitivity of backscattering to humidity was the strongest in BJ, followed by NJ, then GZ, the weakest. With the formation and development of pollution, β_p at all three sites showed enhanced sensitivities to the ambient humidity, but their magnitudes differed (Figure 13). β_p at all three sites increased slightly as the ambient RH increased under clean conditions, partly related to local primary particles with lower hygroscopicity, leading to weak hygroscopic growth. The increase in β_p sharpened with a steeper slope in BJ compared with the gentler slopes in NJ and GZ, particularly under heavily polluted conditions. This is partly caused by the explosive growth of hygroscopic particles that led to heavier pollution periods in BJ. This result demonstrates that ALWC can easily form during polluted periods because there are more highly aged particles, and higher ambient RH can provide enough water for absorption, facilitating aerosol hygroscopic growth and further enhancing the scattering of light by aerosol (Z. Wu et al., 2018).

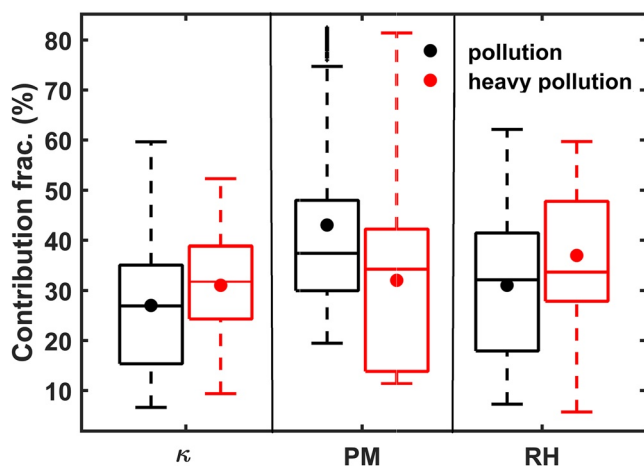


Figure 14. Mean contribution fractions (solid dots) of aerosol hygroscopicity (κ), $\text{PM}_{2.5}$ mass concentration (PM), and ambient relative humidity (RH) to changes in aerosol backscattering coefficient, with boxes showing the 25th, 50th, and 75th percentiles under polluted conditions (black dots and boxes) and heavily polluted conditions (red dots and boxes) in Beijing. Extremities show the 5th and 95th percentiles.

4.3.4. The Contributions of RH, $\text{PM}_{2.5}$, and κ to Variations in β_p

The mean contributions of humidity, particle mass concentration, and chemical composition to variations in backscattering under polluted and heavily polluted conditions are shown for BJ (Figure 14), NJ (Figure 15), and GZ (Figure 16). Note that of the three factors, particle chemical components contributed the least to changes in aerosol backscattering at all three sites

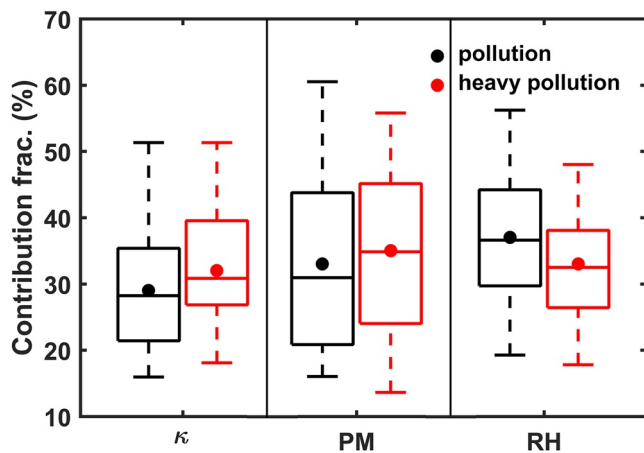


Figure 15. Same as Figure 14 except in Nanjing.

under polluted and heavily polluted conditions. This implies that the particle hygroscopic effect due to the enhancement of aerosol hygroscopicity has a comparatively weaker impact on aerosol backscattering. Overall, the aerosol hygroscopicity, particle mass, and humidity contributed to 27%, 43%, and 30%, respectively, of the changes in β_p in BJ under polluted conditions (Figure 14). This suggests that the accumulation of primary particles had the most significant impact on increasing aerosol backscattering, followed by the aerosol hygroscopic effect, at the beginning stage of pollution in BJ. During this stage, emissions were dominated by primary particles with low hygroscopicity (Figure 8), coupled with low ambient RH conditions (Figure 6). Aerosol hygroscopic growth was consequently weak at the early stage of pollution in BJ. Note that under heavily polluted conditions, pronounced increases in the contributions of RH (37%) and κ (31%) to changes in β_p indicate a significant enhancement of the aerosol hygroscopic growth process with the development of pollution in BJ (Figure 14). This is because high humidity under heavily polluted conditions can supply sufficient moisture for particles dominated by the accumulation mode to absorb, thereby increasing ALWC. This is conducive to the generation of SA and the enhancement of the aerosol hygroscopic effect, further increasing ALWC and finally forming a positive feedback loop. This implies that heavy pollution formation mainly occurs under high ambient RH conditions during winter in BJ. Figure 15 shows that the aerosol hygroscopicity, particle mass concentration, and humidity in NJ contributed to 29%, 33%, and 38% of the changes in β_p under polluted conditions and 32%, 35%, and 33% under heavily polluted conditions, respectively. Generally, opposite to that in BJ, the impact of ambient humidity had the most significant influence on aerosol backscattering, followed by aerosol loading during the initial period of pollution. The influence of the formation of aged particles was the most important during heavily polluted periods in NJ. This is partly related to the high ambient humidity and particle hygroscopicity expected to be affected by aged particles in the early stage of pollution in NJ. The ambient RH in NJ was generally high during pollution formation and development. The explosive growth of NO_3^- through heterogeneous chemical reactions under heavily polluted conditions resulted in a higher contribution of particle concentration to variations in aerosol backscattering. This suggests that the development of pollution is not particularly dependent on ambient humidity and that local emission controls could significantly reduce aerosol backscattering in NJ.

Figure 16 shows the average contributions of the three factors to backscattering under polluted and heavily polluted conditions in GZ. Compared with the other two sites, the fractional contributions of particle hygroscopicity, particle mass concentration, and humidity to changes in β_p differed relatively little between the polluted and heavily polluted conditions, that is, the fractional contributions were 25%, 41%, and 34% under polluted conditions and 23%, 41%, and 36% under heavily polluted conditions, respectively. This suggests that aerosol accumulation had a stronger influence on light scattering than aerosol hygroscopic growth under polluted and heavily polluted conditions, likely because meteorological conditions and aerosol chemical compositions were similar during these two polluted periods in GZ.

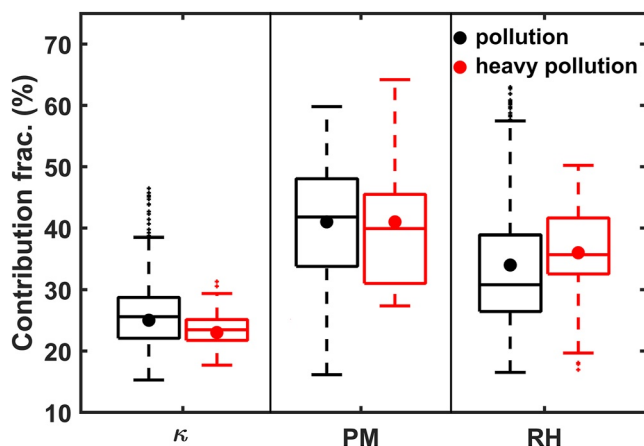


Figure 16. Same as Figure 14 except in Guangzhou.

5. Conclusions

Haze is caused by the scattering of solar radiation by aerosols, which is dictated primarily by aerosol mass loading, size distribution, chemical composition, and meteorology, especially humidity. This study investigates the relationships between aerosol backscattering (β_p), aerosol liquid water content (ALWC), and numerous influential factors [that is, ambient humidity, particle mass concentration, particle number size distribution (PNSD), and chemical composition] using comprehensive field campaign data acquired at three urban sites in China: Beijing (BJ) from 20 December 2018–10 February 2019, Guangzhou (GZ) from 1 November 2019–31 January 2020, and Nanjing (NJ) from 1 November 2020–31 January 2021. The respective roles and contributions of these factors to variations in β_p were examined, quantified, and compared among the three sites. Given that observations were made

during different periods at the three sites, there was no intention to compare their values and seasonal changes. The goal is to understand their differences in terms of underlying physical and chemical processes leading to haze episodes. Identification and quantification of the relative contributions of aerosols and meteorology to the formation of haze are the essential objectives of the study.

Overall, temporal changes in particle backscattering under ambient conditions were consistent with those in aerosol liquid water at the three sites, underlining the significant impact of the particle hygroscopic effect on particle backscattering. On average, β_p in BJ was the strongest ($54 \pm 68 \text{ Mm}^{-1}$), followed by that in NJ ($39 \pm 28 \text{ Mm}^{-1}$) and GZ ($30 \pm 17 \text{ Mm}^{-1}$). The average ALWC in NJ was $39 \pm 110 \mu\text{g m}^{-3}$, much higher than that in BJ ($15 \pm 75 \mu\text{g m}^{-3}$) and GZ ($9 \pm 10 \mu\text{g m}^{-3}$). Related to different local emissions and meteorological factors, there were notable differences between the three sites. The particle mass concentration in BJ was systematically higher than in NJ and GZ, while the ambient RH and aerosol hygroscopicity in NJ were higher than those in BJ and GZ. The significant disparities in particle backscattering and ALWC among the sites were primarily caused by differences in aerosol mass concentration, as indicated by the correlation analyses between backscattering and particle mass concentration, although other factors may dominate under certain circumstances. Backscattering was highly correlated with particle mass concentration in BJ and GZ but poorly correlated in NJ, likely linked to the influence of ALWC. The formation of heavy pollution in BJ was chiefly associated with high humidity, leading to high ALWC and aerosol mass concentrations. Different from BJ, the formation of pollution in NJ was independent of ambient humidity, with a much higher ALWC modeled under both clean and polluted conditions. These results demonstrate the different formation mechanisms of heavy haze between BJ and NJ.

The potential impact of the particle size distribution on backscattering was also evaluated according to Mie scattering theory, showing that the particle size distribution in BJ and NJ had noticeably stronger influences on particle backscattering than in GZ. The influences of humidity and aerosol chemical composition on hygroscopic growth under different pollution conditions at the three sites were also investigated. Sharply enhanced relative humidity (RH) and particle hygroscopicity can significantly influence the size, shape, and chemical composition of aerosol particles through hygroscopic growth.

Distinct differences in the sensitivity of particle backscattering to related factors at the three sites under the same pollution conditions were demonstrated. β_p was more sensitive to aerosol hygroscopicity and mass concentration in NJ than in BJ and GZ and more sensitive to RH in BJ than in NJ and GZ. Finally, differences in the relative contributions of humidity, particle concentration, and aerosol chemical composition to variations in backscattering at the three sites under polluted and heavily polluted conditions were evaluated. Particle hygroscopicity contributed relatively the least to changes in backscattering under all pollution conditions at the three sites. This implies that the particle hygroscopic effect caused by the enhancement of aerosol hygroscopicity had a relatively weaker impact on aerosol backscattering. The largest contributor to the variability in β_p in BJ changed from particle mass under polluted conditions to ambient RH under heavily polluted conditions, implying that the formation of heavy pollution is dependent on high humidity in BJ. The largest contributor to the variability in β_p in NJ changed from ambient RH under polluted conditions to particle concentration under heavily polluted conditions, indicating that the development of pollution is not particularly dependent on the ambient humidity in NJ. There were smaller differences in the contributions of aerosol chemical composition, particle concentration, and humidity to changes in β_p between polluted and heavily polluted conditions in GZ than in the other two sites. Both pollution conditions were dominated by aerosol accumulation, related to similar meteorological and aerosol chemical composition conditions during the two polluted periods. Our results suggest that local control measures taken during severe pollution episodes can efficiently reduce aerosol mass concentrations in NJ and GZ. However, this might not be the case in BJ. This has significant implications for making sound policies in combating air pollution by accounting for the diverse formation mechanisms of heavy haze among the three sites.

Conflict of Interest

The authors declare no conflicts of interest relevant to this study.

Data Availability Statement

Aurora-3000, ACSM, and SMPS datasets can be downloaded from the following link: <http://dx.doi.org/10.17632/ryjfh4dn5.1> (X. Jin, 2022). In situ measurements can be downloaded from the following link: <https://www.aqis-tudy.cn/> (China MEP, 2013).

Acknowledgments

This study was funded by the National Natural Science Foundation of China (Grant 42030606), the Guangdong Basic and Applied Basic Research Fund (Grant 2020B1515130003), and the ZAFU Scientific Research Development Foundation (Grant2022LFR084).

References

- Bian, Y. X., Zhao, C. S., Ma, N., Chen, J., & Xu, W. Y. (2014). A study of aerosol liquid water content based on hygroscopicity measurements at high relative humidity in the North China Plain. *Atmospheric Chemistry and Physics*, *14*(12), 6417–6426. <https://doi.org/10.5194/acp-14-6417-2014>
- Bohren, C. F., & Huffman, D. R. (2007). Absorption and scattering by an arbitrary particle. In *Absorption and Scattering of Light by Small Particles* (pp. 57–81). Wiley-VCH.
- Chen, J., Zhao, C. S., Ma, N., & Yan, P. (2014). Aerosol hygroscopicity parameter derived from the light scattering enhancement factor measurements in the North China Plain. *Atmospheric Chemistry and Physics*, *14*(15), 8105–8118. <https://doi.org/10.5194/acp-14-8105-2014>
- Cheng, Y. F., Wiedensohler, A., Eichler, H., Heintzenberg, J., Tesche, M., Ansmann, A., et al. (2008). Relative humidity dependence of aerosol optical properties and direct radiative forcing in the surface boundary layer at Xinken in Pearl River Delta of China: An observation based numerical study. *Atmospheric Environment*, *42*(25), 6373–6397. <https://doi.org/10.1016/j.atmosenv.2008.04.009>
- China MEP (Ministry of Environmental Protection, China). (2013). Online monitoring and analysis platform of China air Quality [Dataset]. China MEP. Retrieved from <https://quotsoft.net/air>
- Covert, D. S., Charlson, R. J., & Ahlquist, N. C. (1972). A study of the relationship of chemical composition and humidity to light scattering by aerosols. *Journal of the Applied Meteorology and Climatology*, *11*(6), 968–976. [https://doi.org/10.1175/1520-0450\(1972\)011<0968:ASOTRO>2.0.CO;2](https://doi.org/10.1175/1520-0450(1972)011<0968:ASOTRO>2.0.CO;2)
- Cui, J., Shi, T., Zhou, Y., Wu, D., Wang, X., & Pu, W. (2021). Satellite-based radiative forcing by light-absorbing particles in snow across the Northern Hemisphere. *Atmospheric Chemistry and Physics*, *21*(1), 269–288. <https://doi.org/10.5194/acp-21-269-2021>
- Fan, M. Y., Zhang, Y. L., Lin, Y. C., Li, L., Xie, F., Hu, J., & Cao, F. (2021). Source apportionments of atmospheric volatile organic compounds in Nanjing, China during high ozone pollution season. *Chemosphere*, *263*, 128025. <https://doi.org/10.1016/j.chemosphere.2020.128025>
- Fountoukis, C., & Nenes, A. (2007). Isorropia II: A computationally efficient thermodynamic equilibrium model for K^+ - Ca^{2+} - Mg^{2+} - NH_4^+ - Na^+ - $SONO-Cl$ - H_2O aerosols. *Atmospheric Chemistry and Physics*, *7*(17), 4639–4659. <https://doi.org/10.5194/acp-7-4639-2007>
- Gysel, M., Grosier, J., Topping, D. O., Whitehead, J. D., Bower, J. N., Cubison, M. J., et al. (2007). Closure study between chemical composition and hygroscopic growth of aerosol particles during TORCH2. *Atmospheric Chemistry and Physics*, *7*(24), 6131–6144. <https://doi.org/10.5194/acp-7-6131-2007>
- Hegg, D. A., Covert, D. S., Crahan, K., & Jonsson, H. (2002). The dependence of aerosol light-scattering on RH over the Pacific Ocean. *Geophysical Research Letters*, *29*(8), 1219. <https://doi.org/10.1029/2001GL014495>
- Huang, J., & Yi, Y. (1991). Inversion of a nonlinear dynamical model from the observation. *Science in China, Series B*, *10*(34), 1246.
- IPCC. (2013). *Climate change 2013: Scientific basis, Fifth Assessment of the Inter-governmental panel on climate change*. Cambridge University Press.
- Jimenez, J. L., Jayne, J. T., Shi, Q., Kolb, C. E., Worsnop, D. R., Yourshaw, I., & Morris, J. W. (2003). Ambient aerosol sampling using the aerodyne aerosol mass spectrometer. *Journal of Geophysical Research*, *108*(D7), 8425. <https://doi.org/10.1029/2001JD001213>
- Jin, X. (2022). “Differentiating the contributions of particle concentration, humidity, and hygroscopicity to scattering of light by aerosol at three sites in China”. V2 [Dataset]. Mendeley Data. <https://doi.org/10.17632/ryjfh4dn5.1>
- Jin, X., Li, Z., Wu, T., Wang, Y., Cheng, Y., Su, T., et al. (2022). The different sensitivities of aerosol optical properties to particle concentration, humidity, and hygroscopicity between the surface level and the upper boundary layer in Guangzhou, China. *Sciences of the Total Environment*, *803*, 150010. <https://doi.org/10.1016/j.scitotenv.2021.150010>
- Jin, X., Wang, Y., Li, Z., Zhang, F., Xu, W., Sun, Y., et al. (2020). Significant contribution of organics to aerosol liquid water content in winter in Beijing, China. *Atmospheric Chemistry and Physics*, *20*(2), 901–914. <https://doi.org/10.5194/acp-20-901-2020>
- Kuang, Y., Zhao, C. S., Tao, J. C., Bian, Y. X., & Ma, N. J. A. E. (2016). Impact of aerosol hygroscopic growth on the direct aerosol radiative effect in summer on North China Plain. *Atmospheric Environment*, *147*, 224–233. <https://doi.org/10.1016/j.atmosenv.2016.10.013>
- Kuwata, M., & Martin, S. T. (2012). Phase of atmospheric secondary organic material affects its reactivity. *Proceedings of the National Academy of Sciences of the U. S. A.*, *109*(43), 17354–17359. <https://doi.org/10.1073/pnas.1209071109>
- Levin, E. J. T., Prenni, A. J., Palm, B. B., Day, D. A., Campuzano-Jost, P., Winkler, P. M., et al. (2014). Size-resolved aerosol composition and its link to hygroscopicity at a forested site in Colorado. *Atmospheric Chemistry and Physics*, *14*(5), 2657–2667. <https://doi.org/10.5194/acp-14-2657-2014>
- Li, Z., Lau, W. M., Ramanathan, V., Wu, G., Ding, Y., Manoj, M. G., et al. (2016). Aerosol and monsoon climate interactions over Asia. *Reviews of Geophysics*, *54*(4), 866–929. <https://doi.org/10.1002/2015RG000500>
- Li, Z., Wang, Y., Guo, J., Zhao, C., Cribb, M. C., Dong, X., et al. (2019). East Asian study of tropospheric aerosols and their impact on regional clouds, precipitation, and climate (EAST-AIRCPC). *Journal of Geophysical Research: Atmospheres*, *124*(23), 13026–13054. <https://doi.org/10.1029/2019JD030758>
- Lin, Z. J., Zhang, Z. S., Zhang, L., Tao, J., Zhang, R. J., Cao, J. J., et al. (2014). An alternative method for estimating hygroscopic growth factor of aerosol light-scattering coefficient: A case study in an urban area of Guangzhou, south China. *Atmospheric Chemistry and Physics*, *14*, 7631–7644. <https://doi.org/10.5194/acp-14-7631-2014>
- Liu, J., Ren, C., Huang, X., Nie, W., Wang, J., Sun, P., et al. (2020). Increased aerosol extinction efficiency hinders visibility improvement in eastern China. *Geophysical Research Letters*, *47*(20), e2020GL090167. <https://doi.org/10.1029/2020GL090167>
- Liu, X., Cheng, Y., Zhang, Y., Jung, J., Sugimoto, N., Chang, S., et al. (2008). Influences of relative humidity and particle chemical composition on aerosol scattering properties during the 2006 PRD campaign. *Atmospheric Environment*, *42*(7), 1525–1536. <https://doi.org/10.1016/j.atmosenv.2007.10.077>
- Ma, N., Zhao, C., Chen, J., Xu, W., Yan, P., & Zhou, X. (2014). A novel method for distinguishing fog and haze based on $PM_{2.5}$, visibility, and relative humidity. *Science China: Earth Sciences*, *57*(9), 2156–2164. <https://doi.org/10.1007/s11430-014-4885-5>

- Malm, W. C., McMeeking, G. R., Kreidenweis, S. M., Levin, E., Carrico, C. M., Day, D. E., et al. (2009). Using high time resolution aerosol and number size distribution measurements to estimate atmospheric extinction. *Journal of the Air and Waste Management Association*, 59(9), 1049–1060. <https://doi.org/10.3155/1047-3289.59.9.1049>
- McMurry, P. H. (2000). A review of atmospheric aerosol measurements. *Atmospheric Environment*, 34(12–14), 1959–1999. [https://doi.org/10.1016/S1352-2310\(99\)00455-0](https://doi.org/10.1016/S1352-2310(99)00455-0)
- Mei, F., Hayes, P. L., Ortega, A., Taylor, J. W., Allan, J. D., Gilman, J., et al. (2013). Droplet activation properties of organic aerosols observed at an urban site during CalNex-LA. *Journal of Geophysical Research: Atmospheres*, 118(7), 2903–2917. <https://doi.org/10.1002/jgrd.50285>
- Ng, N. L., Herndon, S. C., Trimborn, A., Canagaratna, M. R., Croteau, P. L., Onasch, T. B., et al. (2011). An aerosol chemical speciation monitor (ACSM) for routine monitoring of the composition and mass concentrations of ambient aerosol. *Aerosol Science & Technology*, 45(7), 780–794. <https://doi.org/10.1080/02786826.2011.560211>
- Nguyen, T. K. V., Zhang, Q., Jimenez, J. L., Pike, M., & Carlton, A. G. (2016). Liquid water: Ubiquitous contributor to aerosol mass. *Environmental Science and Technology Letters*, 3(7), 257–263. <https://doi.org/10.1021/acs.estlett.6b00167>
- Pan, Y., Tian, S., Liu, D., Fang, Y., Zhu, X., Gao, M., et al. (2018). Source apportionment of aerosol ammonium in an ammonia-rich atmosphere: An isotopic study of summer clean and hazy days in urban Beijing. *Journal of Geophysical Research: Atmospheres*, 123(10), 5681–5689. <https://doi.org/10.1029/2017JD028095>
- Peters, M. D., & Kreidenweis, S. M. (2007). A single parameter representation of hygroscopic growth and cloud condensation nucleus activity. *Atmospheric Chemistry and Physics*, 7(8), 1961–1971. <https://doi.org/10.5194/acp-7-1961-2007>
- Pierangelo, C., Chedin, A., Heilliette, S., Jacquinet-Husson, N., & Armante, R. (2004). Dust altitude and infrared optical depth from AIRS. *Atmospheric Chemistry and Physics*, 4(7), 1813–1822. <https://doi.org/10.5194/acp-4-1813-2004>
- Ren, R., Li, Z., Yan, P., Wang, Y., Wu, H., Cribb, M. C., et al. (2021). The effect of aerosol chemical composition on light scattering due to the hygroscopic swelling effect. *Atmospheric Chemistry and Physics*, 21(13), 9977–9994. <https://doi.org/10.5194/acp-21-9977-2021>
- Seinfeld, H. J., & Pandis, N. S. (2006). *Atmospheric chemistry and Physics: From air pollution to climate change*. John Wiley & Sons. <https://doi.org/10.1080/00139157.1999.10544295>
- Seinfeld, J. H., & Pandis, S. N. (1998). From air pollution to climate change. *Atmospheric Chemistry and Physics*, 1326.
- Stocker, D. Q., Qin, D., Plattner, G.-K., Tignor, M., Allen, S. K., Boschung, J., et al. (2013). Climate change 2013: The physical science basis. In *Working Group I Contribution to the Fifth Assessment Report of the Intergovernmental Panel on Climate Change Summary for Policymakers*. IPCC.
- Stokes, R. H., & Robinson, R. A. (1966). Interactions in aqueous nonelectrolyte solutions. I. Solute-solvent equilibria. *Journal of Physical Chemistry*, 70(7), 2126–2131. <https://doi.org/10.1021/j100879a010>
- Su, T., Li, Z., Li, C., Li, J., Han, W., Shen, C., et al. (2020). The significant impact of aerosol vertical structure on lower atmosphere stability and its critical role in aerosol–planetary boundary layer (PBL) interactions. *Atmospheric Chemistry and Physics*, 20(6), 3713–3724. <https://doi.org/10.5194/acp-20-3713-2020>
- Su, T., Li, Z., Zheng, Y., Luan, Q., & Guo, J. (2020). Abnormally shallow boundary layer associated with severe air pollution during the COVID-19 lockdown in China. *Geophysical Research Letters*, 47(20), e2020GL090041. <https://doi.org/10.1029/2020GL090041>
- Sun, Y., Wang, Z., Dong, H., Yang, T., Li, J., Pan, X., et al. (2012). Characterization of summer organic and inorganic aerosols in Beijing, China with an aerosol chemical speciation monitor. *Atmospheric Environment*, 51, 250–259. <https://doi.org/10.1016/j.atmosenv.2012.01.013>
- Tan, H., Cai, M., Fan, Q., Liu, L., Li, F., Chan, P. W., et al. (2017). An analysis of aerosol liquid water content and related impact factors in Pearl River Delta. *Science of the Total Environment*, 579, 1822–1830. <https://doi.org/10.1016/j.scitotenv.2016.11.167>
- Tao, J. C., Zhao, C. S., Ma, N., & Liu, P. F. (2014). The impact of aerosol hygroscopic growth on the single-scattering albedo and its application on the NO₂ photolysis rate coefficient. *Atmospheric Chemistry and Physics*, 14(22), 12055e12067. <https://doi.org/10.5194/acp-14-12055-2014>
- Topping, D. O., McFiggans, G. B., & Coe, H. (2005). A curved multi-component aerosol hygroscopicity model framework: Part 1 – Inorganic compounds. *Atmospheric Chemistry and Physics*, 5(5), 1205–1222. <https://doi.org/10.5194/acp-5-1205-2005>
- Volkamer, R., San Martini, F., Molina, L. T., Salcedo, D., Jimenez, J. L., & Molina, M. J. (2007). A missing sink for gas-phase glyoxal in Mexico city: Formation of secondary organic aerosol. *Geophysical Research Letters*, 34(19), L19807. <https://doi.org/10.1029/2007GL030752>
- Wang, T., Nie, W., Gao, J., Xue, L. K., Gao, X. M., Wang, X. F., et al. (2010). Air quality during the 2008 Beijing Olympics: Secondary pollutants and regional impact. *Atmospheric Chemistry and Physics*, 10(16), 7603–7615. <https://doi.org/10.5194/acp-10-7603-2010>
- Wang, Y., Zhang, F., Li, Z., Tan, H., Xu, H., Ren, J., et al. (2017). Enhanced hydrophobicity and volatility of submicron aerosols under severe emission control conditions in Beijing. *Atmospheric Chemistry and Physics*, 17(8), 5239–5251. <https://doi.org/10.5194/acp-17-5239-2017>
- Wex, H., Petters, M. D., Carrico, C. M., Hallbauer, E., Massling, A., McMeeking, G. R., et al. (2009). Towards closing the gap between hygroscopic growth and activation for secondary organic aerosol: Part 1 – Evidence from measurements. *Atmospheric Chemistry and Physics*, 9(12), 3987–3997. <https://doi.org/10.5194/acp-9-3987-2009>
- Whitby, K. T. (1978). The physical characteristics of sulfur aerosols. *Atmospheric Environment*, 12(1–3), 135–159. [https://doi.org/10.1016/0004-6981\(78\)90196-8](https://doi.org/10.1016/0004-6981(78)90196-8)
- Wu, T., Li, Z., Jin, X., Wu, H., Ren, R., Zhang, D., et al. (2022). LiDAR-based remote sensing of the vertical profile of aerosol liquid water content using a machine-learning model. *IEEE Transactions on Geosciences and Remote Sensing*, 60, 1–10. <https://doi.org/10.1109/TGRS.2021.3130204>
- Wu, Z., Wang, Y., Tan, T., Zhu, Y., Li, M., Shang, D., et al. (2018). Aerosol liquid water driven by anthropogenic inorganic salts: Implying its key role in the haze formation over North China plain. *Environmental Science and Technology Letters*, 5(3), 160–166. <https://doi.org/10.1021/acs.estlett.8b00021>
- Wu, Z. J., Zheng, J., Shang, D. J., Du, Z. F., Wu, Y. S., Zeng, L. M., et al. (2016). Particle hygroscopicity and its link to chemical composition in the urban atmosphere of Beijing, China, during summertime. *Atmospheric Chemistry and Physics*, 16(2), 1123–1138. <https://doi.org/10.5194/acp-16-1123-2016>
- Xu, W., Kuang, Y., Bian, Y., Liu, L., Li, F., Wang, Y., et al. (2020). Current challenges in visibility improvement in southern China. *Environmental Science and Technology Letters*, 7(6), 395–401. <https://doi.org/10.1021/acs.estlett.0c00274>
- Xue, J., Yuan, Z., Griffith, S. M., Yu, X., Lau, A. K., & Yu, J. (2016). Sulfate formation enhanced by a cocktail of high NO_x, SO₂, particulate matter, and droplet pH during haze-fog events in megacities in China: An observation-based modeling investigation. *Environmental Science and Technology*, 50(14), 7325–7334. <https://doi.org/10.1021/acs.est.6b00768>
- Yang, S., Li, X., Song, M., Liu, Y., Yu, X., Chen, S., et al. (2021). Characteristics and sources of volatile organic compounds during pollution episodes and clean periods in the Beijing-Tianjin-Hebei region. *Science of the Total Environment*, 799, 149491. <https://doi.org/10.1016/j.scitotenv.2021.149491>
- Yoon, S. C., & Kim, J. (2006). Influences of relative humidity on aerosol optical properties and aerosol radiative forcing during ACE-Asia. *Atmospheric Environment*, 40(23), 4328–4338. <https://doi.org/10.1016/j.atmosenv.2006.03.036>

- Zhang, D., Li, Z., Wu, H., Wu, T., Ren, R., Cai, Z., et al. (2022). Analysis of aerosol particle number size distribution and source attribution at three megacities in China. *Atmospheric Environment*, 279, 119114. <https://doi.org/10.1016/j.atmosenv.2022.119114>
- Zhang, F., Li, Y., Li, Z., Sun, L., Li, R., Zhao, C., et al. (2014). Aerosol hygroscopicity and cloud condensation nuclei activity during the AC³Exp campaign: Implications for cloud condensation nuclei parameterization. *Atmospheric Chemistry and Physics*, 14(24), 13423–13437. <https://doi.org/10.5194/acp-14-13423-2014>
- Zhang, F., Wang, Y., Peng, J., Ren, J., Collins, D., Zhang, R., et al. (2017). Uncertainty in predicting CCN activity of aged and primary aerosols. *Journal of Geophysical Research: Atmospheres*, 122(21), 11723–11736. <https://doi.org/10.1002/2017JD027058>
- Zhang, L., Cao, X., Bao, J., Zhou, B., Huang, J., Shi, J., & Bi, J. (2010). A case study of dust aerosol radiative properties over Lanzhou, China. *Atmospheric Chemistry and Physics*, 10(9), 4283–4293. <https://doi.org/10.5194/acp-10-4283-2010>
- Zhang, X. Q., & McMurry, P. H. (1993). Evaporative losses of fine particulate nitrates during sampling. *Atmospheric Environment*, 26A(18), 3305–3312. [https://doi.org/10.1016/0960-1686\(92\)90347-N](https://doi.org/10.1016/0960-1686(92)90347-N)
- Zhang, Y., Sun, Y., Du, W., Wang, Q., Chen, C., Han, T., et al. (2016). Response of aerosol composition to different emission scenarios in Beijing, China. *Science of the Total Environment*, 571, 902–908. <https://doi.org/10.1016/j.scitotenv.2016.07.073>
- Zhao, P., Xiao, H., Liu, J., & Zhou, Y. (2022). Precipitation efficiency of cloud and its influencing factors over the Tibetan plateau. *International Journal of Climatology*, 42(1), 416–434. <https://doi.org/10.1002/joc.7251>
- Zieger, P., Väisänen, O., Corbin, J. C., Partridge, D. G., Bastelberger, S., Mousavi-Fard, M., et al. (2017). Revising the hygroscopicity of inorganic sea salt particles. *Nature Communications*, 8(1), 15883. <https://doi.org/10.1038/ncomms15883>